Synthesis, Rietveld refinements and electrical conductivity of news fluorobritholite based on lead Ca 7-x Pb x La 3 (PO 4) 3 (SiO 4) 3 F 2 (0 ≤ x ≤ 2)

S. Ben Moussa, M. Laajimi, R Ben Chaâbane, B. Badraoui, M. Gruselle, A. Laghzizil

Synthesis, Rietveld refinements and electrical conductivity of news fluorobritholite based on lead $Ca_{7-x}Pb_xLa_3(PO_4)_3(SiO_4)_3F_2$ ($0 \leq x \leq 2$)

S. Ben Moussa [1], M. Laajimi [2], R. Ben Chaâbane [2], B. Badraoui [1*], M.Gruselle [3], A. Laghzizil [4]

[1] *U.R. Matériaux et synthèse organique UR17ES31, Institut Préparatoire aux Etudes d'Ingénieur de Monastir, Université de Monastir, 5019 Monastir, Tunisia*
[2] *Laboratoire des Interfaces et Matériaux Avancés, Faculté des Sciences de Monastir, Boulevard de l'Environnement, Université de Monastir, 5019 Monastir, Tunisia*
[3] *Sorbonne Université, UPMC Univ Paris 06, CNRS, UMR 8232, Institut Parisien de Chimie Moléculaire, F-75005 Paris, France*
[4] *Laboratoire de Chimie Physique Générale, Université Mohammed V, Av. Ibn Batouta BP1014, Rabat, Morocco*

Abstract

Fluorobritholites of general formula $Ca_{7-x}Pb_xLa_3(PO_4)_3(SiO_4)_3F_2$, ($0 \leq x \leq 2$) were prepared by thermal method. The obtained solid solutions were characterized by X-Ray diffraction, infrared spectroscopy and chemical analysis. The structural refinement carried out via the Rietveld method provides evidence that La^{3+} and Pb^{2+} substituting Ca^{2+} ions are located into the two cationic sites with a strong preference for metal M(2) sites. A progressive shift of the F^- ion toward the center of the triangles formed by the site M(2) metals has been observed when the lead content increased. The electrical conductivity of the fluorobritholite materials depends on the applied frequency (100 Hz – 10 MHz) by means of the complex impedance spectroscopy. The effect of Pb and La-substitution on the conductivity properties of the studied fluorobritholites is correlated with Pb content. The carriers that govern the conductivity are: the nature of the welcome sites and the dimension of the tunnels.

Keywords: Fluorobritholite, Rare earths, Rietveld refinement, Ionic conductivity

1. Introduction

Recently, there have been many reports on the synthesis and characterization of fluorobritholites, but there are very few reports on their conduction properties [1-3]. Fluorobritholites belongs to the very large family of apatites.

Apatites are the most abundant minerals on Earth, attracting much attention for their potential applications such as catalysts [4], sensors [5], luminescence [6], ionic exchangers and biomaterials [7]. The fluoroapatite, $Ca_{10}(PO_4)_6F_2$ (fig.1) is considered as a good structural model for apatitic compounds with space group P63/m [8,9].

The multifunctionnality of calcium apatites is correlated to the large capability for element substitution by changes in the anionic and cationic composition. The substitution of calcium by bivalent metals (Sr, Ba, Pb) [10,11], and monovalent (Na, K, Li) affects the fluoride mobility in apatite tunnels [12-14]. The limit of miscibility for these systems was correlated with the relative properties of the metals, such as polarizability, electronegativity and cationic size.

Fluorobritholite, rare-earth phosphosilicates, resulting from the substitution of the divalent cation by a trivalent rare earth element and the trivalent XO_4 group by the silicate tetravalent group (SiO_4), has attracted researchers interest to their potential use as oxide ion conductors or confinement matrices for the minor actinides and long-lived fission products [15-17]. Several studies have shown that the performance of these materials to store nuclear waste decreases with the increase of SiO_4 groups substituting PO_4 ones and the decrease of the fluorine content in the apatite framework [18,19]. The stability of Fluorobritholites of general formula $M_{10-x}La_x(PO_4)_{6-x}(SiO_4)_xF_2$ (M= Ca, Sr) and $Sr_{7-x}Ca_xLa_3(PO_4)_3(SiO_4)_3F_2$ [2,20] decrease with the increase of the substitution degree and the La atoms preferentially occupy the (6 h) sites into the apatitic structure. The incorporation of La^{3+} and SiO_4^{4-} ions into the apatite structure affects the crystalline parameters and limits the metal substitution in apatite structure.

Because of the strong interaction between ionic conduction and its environment, the electrical properties of fluorobritholite, $Ca_{7-x}Pb_xLa_3(PO_4)_3(SiO_4)_3F_2$, has been investigated highlighting the key role played by the metal substitution on fluoride mobility in fluorobritholite ceramics.

In this article, we describe the synthesis and characterization of $Ca_{7-x}Pb_xLa_3(PO_4)_3(SiO_4)_3F_2$ solid solutions. The nature of charge transport in these solids was investigated using Impedance Spectroscopy which is a powerful technique for exploring the charge carrier transport and relaxation processes.

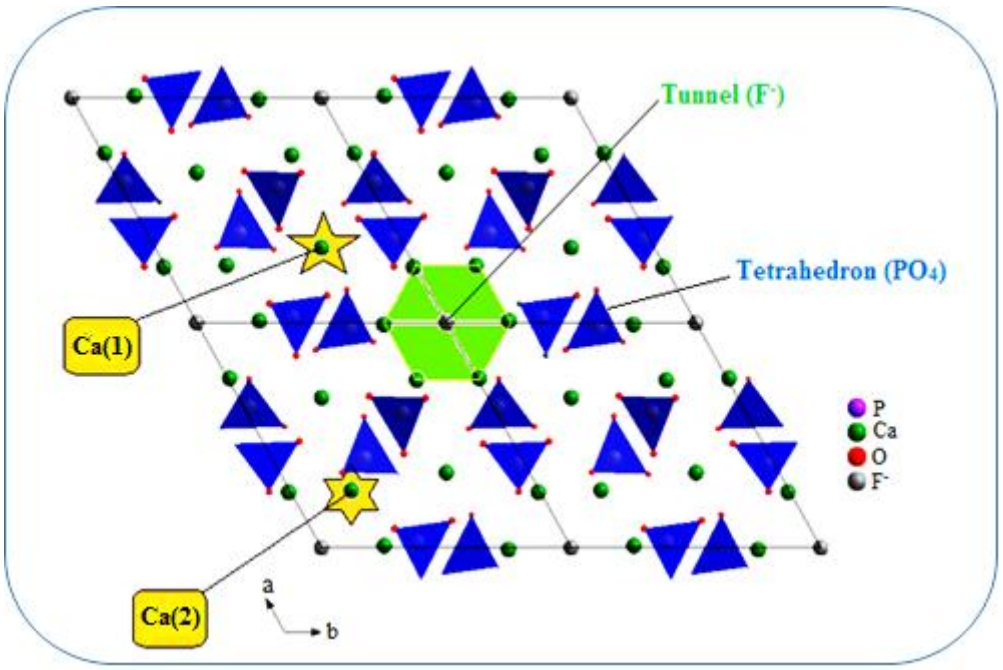

Figure 1. Crystal structure of $Ca_{10}(PO_4)_6F_2$.

2. Materials and methods

. *Preparation of intermediary calcium biphosphate precursor*

To have a single apatite phase without any second phase, the calcium diphosphate $Ca_2P_2O_7$ is employed as intermediary precursor for fluorobritholite $Ca_{7-x}Pb_xLa_3(PO_4)_3(SiO_4)_3F_2$ synthesis. The $Ca_2P_2O_7$ are obtained by a stoichiometric mixture of calcium carbonate ($CaCO_3$) (99.0% Fluka) and diammonium hydrogen phosphate ($(NH_4)_2HPO_4$) (>99% Acros organics). These reagents were thoroughly ground in an agate mortar and pressed into pellets and heat-treated under an argon flow at 900°C for 12 h according to the following reaction:

$$\begin{matrix} NH_4 \quad {}_2HPO_4 \rightarrow Ca_2P_2O_7 + 4NH_3(\uparrow) + 2CO_2(\uparrow) + 3H_2O(\uparrow) \\ 2CaCO_3 + 2 \end{matrix}$$

.*Synthesis of $Ca_{7-x}Pb_xLa_3(PO_4)_3(SiO_4)_3F_2$ solid solution*

The reagents $PbCO_3$ (98% Labochimie), CaF_2 (98.2% Prolabo), SiO_2 (>99.5% Alfa), La_2O_3 (>99.5% Prolabo), and $Ca_2P_2O_7$ were taken under stoichiometric conditions according to following equation:

$$CaF_2 + (3-x)CaCO_3 + \frac{3}{2}Ca_2P_2O_7 + xPbCO_3 + \frac{3}{2}La_2O_3 + 3SiO_2 \rightarrow Ca_{(7-x)}Pb_xLa_3(PO_4)_3(SiO_4)_3F_2 + 3CO_2(\uparrow)$$

After being closely mixed in an agate mortar, the reagents were pressed cold into pellets 12 mm in diameter. Then, they underwent two thermal treatments under dynamic argon atmosphere. The first treatment was carried out at 900°C during 12 hours, which was aimed to evacuate the decomposition products, whereas the second one took place at a temperature ranging from 1200 to 1400°C with a heating rate of 10 °C/min. In the following sections, the compositions with x=0, 1 and 2 will be labeled as Ca_7La_3FAp, $Ca_6Pb_1La_3FAp$ and $Ca_5Pb_2La_3FAp$, respectively.

. *Techniques of characterisation*

X-ray diffraction analysis was carried out by means of a X'Pert Pro PANalytical diffractometer using Cu Kα radiation (λ=1.5418 Å), with θ-θ geometry, equipped with an X'Celerator solid detector and a Ni filter. The data were collected in a 2θ range from 10° to 70°, with a step size of 0.02° and a scanning step time of 10 s. The crystalline phase identification was done by comparing the experimental XRD patterns to the standards compiled by the Joint Committee on Powder Diffraction and Standards (JCPDS). Rietveld refinements [21] of the samples were carried out with FULLPROF program [22] using the fluorapatite data as starting parameters [23]. For the refinements, the background was estimated by a fifth-degree polynom, and the peak shapes were modelled using a Pseudo-Voigt function. Infrared absorption spectroscopy was performed using a Spectrum Two 104462 IR spectrophotometer equipped with a diamond ATR setup in the range 4000-400 cm^{-1}. The amounts of Ca, Pb and La were determined using an atomic absorption spectrophotometer (Perkin-Elmer 3110). The phosphate ions were analyzed by

a UV-visible absorption spectrophotometry using phosphovanadomolybdic complex. For the electrical measurements, All electrodes were of aluminium deposited on to the both surface of pellets using evaporation of aluminium under high vacuum and heated at 600°C to favor the adhesion process (ceramic-electrode). The conductance frequency's dependence is investigated using HP 4192A impedance analyser in the frequency range between 100Hz and 10MHz. All electrical measurement are performed at room temperature (T= 23°C) with relative humidity of 55%.

Results and discussion

3.1. Chemical analysis

The results of the chemical analysis are summarized in Table 1. The contents of the different elements in the resulting products were closed to those expected based on the stoichiometry of the starting materials. The atomic ratios (Ca+Pb+La)/(P+Si) are close to the stoichiometric value of 1.667 for steochiometric fluorapatite.

Table 1

Chemical composition of samples (atoms per unit cell)

	Ca	Pb	La	P	Si	F	(Ca+Pb+La)/(P+Si)
Ca_7La_3FAp	6.99(2)	0	3.00(4)	2.99(3)	3.02(4)	1.97(5)	1.662(4)
$Ca_6Pb_1La_3FAp$	6.01(3)	0.98(3)	2.98(2)	3.01(3)	3.00(3)	1.96(4)	1.664(5)
$Ca_5Pb_2La_3FAp$	4.99(3)	2.01(1)	3.01(4)	3.00(1)	2.99(2)	2.01(5)	1.671(3)

3.2. X-ray analysis

The X-ray diffraction patterns of the samples $Ca_6Pb_1La_3(PO_4)_3(SiO_4)_3F_2$ and $Ca_5Pb_2La_3(PO_4)_3(SiO_4)_3F_2$ are shown in Figure 2. All peaks of each pattern were indexed in the hexagonal system with space group $P6_3/m$ based on the fluorapatite pattern (JCPDS 00-071-0880). No secondary phases were detected in any of the patterns. Rietveld refinement was performed in several stages, the parameters obtained in each stage being deferred in the

following. Then, the refined parameters were used as an initial model for the apatite with lead content immediately lower, and so on. The X-ray scattering factors for Ca^{2+}, Pb^{2+}, La^{3+}, O^{2-} ions and for the P and Si atoms were used. Detailed results of the structural refinements are grouped in Table 2. In this table, are also reported the residuals for the weighted pattern R_{wp}, the pattern R_p, the structure factor R_F, the Bragg factor R_F, the goodness of fit χ^2 and the number of molecules per unit cell Z.

Figure 2. Experimental and calculated X-ray diffraction patterns of (a) $Ca_6Pb_1La_3FAp$ and (b) $Ca_5Pb_2La_3FAp$.

Table 2

Lattice parameters (Å), agreement indexes and fractional atomic coordinates after Rietveld refinement for the mixed $Ca_{7-x}Pb_xLa_3FAp$ (e.s.d. in parentheses)

$Ca_6Pb_1La_3FAp$		**a=9.5493(1)**	**c=7.0263(9)**	**Z =1**		
	R_p= 7.12	R_{wp}= 7.69	R_B= 3.18	R_F = 1.98		χ^2 = 3.28
Atom	M	x	y	z	occupancy factors	B(Å)^2
P/Si	6h	0.4023(3)	0.3709(3)	0.25000	0.249(9)	0.86(6)
Ca(1)	4f	0.33333	0.66667	0.0023(4)	0.232(2)	1.25(2)
Pb(1)	4f	0.33333	0.66667	0.0022(8)	0.001(2)	1.25(2)
La(1)	4f	0.33333	0.66667	0.0022(8)	0.067(6)	1.25(2)
Ca(2)	6h	0.2374(1)	-0.0108(6)	0.25000	0.267(7)	1.25(2)
Pb(2)	6h	0.2374(1)	-0.0108(6)	0.25000	0.082(3)	1.25(2)
La(2)	6h	0.2374(1)	-0.0108(6)	0.25000	0.182(3)	1.25(2)
O(1)	6h	0.3346(6)	0.4964(1)	0.25000	0.500	2.08(8)
O(2)	6h	0.5844(8)	0.4632(7)	0.25000	0.500	2.08(8)
O(3)	12i	0.3422(5)	0.2567(3)	0.0711(6)	1.000	2.08(8)
F	4e	0.00000	0.00000	0.2022(2)	0.167	0.13(4)
$Ca_5Pb_2La_3FAp$		**a=9.5520(9)**	**c=7.0296(1)**	**Z =1**		
	R_p= 8.48	R_{wp}= 9.32	R_B = 3.96	R_F = 2.92		χ^2 = 4.74
P/Si	6h	0.4029(4)	0.3722(9)	0.25000	0.244(1)	1.10(7)
Ca(1)	4f	0.33333	0.66667	0.0003(8)	0.191 (7)	1.21(2)
Pb(1)	4f	0.33333	0.66667	0.0003(8)	0.015(2)	1.21(2)
La(1)	4f	0.33333	0.66667	0.0003(8)	0.074(8)	1.21(2)
Ca(2)	6h	0.2362(8)	-0.0117(8)	0.25000	0.224(8)	1.21(2)
Pb(2)	6h	0.2362(8)	-0.0117(8)	0.25000	0.151(3)	1.21(2)
La(2)	6h	0.2362(8)	-0.0117(8)	0.25000	0.175(1)	1.21(2)
O(1)	6h	0.3401(8)	0.4934(2)	0.25000	0.500	2.35(1)
O(2)	6h	-0.1251(5)	0.4210(8)	0.25000	0.500	2.35(1)
O(3)	12i	0.0819(5)	0.3475(9)	-0.0792(6)	1.000	2.35(1)
F	4e	0.00000	0.00000	0.21661(1)	0.167	0.34(3)

The progressive substitution of calcium by lead provides a slight increase in the lattice parameters *(a, c)* related to the difference in size between these metals (Pb^{2+} coord. 7, radius 1.37 Å; Ca^{2+} coord. 7, radius 1.2 Å) [24] . Several studies have analyzed the occupancy of lanthanide ions between the two crystallographic sites in the apatitic structure. Several works indicate that the La atoms are distributed between the two crystallographic sites M(1) and M(2) in apatite structure, with a clear preference for the larger site M(2), demonstrating that the nature of the

channel anion plays a significant role in the distribution of La^{3+} between the two cationic sites [25,26]. Furthermore, Ardhaoui et al. [27,28] indicated that the introduction of La^{3+} in the apatite structure has a strong influence on its stability. The Table 3 gathers the refinement of the occupation factors indicates that the tree metallic ions Ca^{2+}, Pb^{2+} and La^{3+}which are distributed between the two crystallographic sites M(1) and M(2), with preference for Pb and La in M(2) sites. In $Ca_6Pb_1La_3FAp$, Pb occupies exclusively the M(2) sites (99%) higher than that occupied for $Ca_5Pb_2La_3FAp$ (90%). For Ca_7La_3FAp sample (x=0), lanthanum occupies 85% of the six-fold sites M(2) and 15% of the four-fold M(1) sites, where the preference is maintained and its occupancy decreased to 73% in $Ca_6Pb_1La_3FAp$ and to 70% in $Ca_5Pb_2La_3FAp$. To explain this localization, other properties such as electronegativity and/or polarizability have been invoked. In mixed Ca and La atoms have approximately the same ionic radii and electronegativity, but their polarisabilities are different, however, Ca and Pb atoms have the same charge, whereas ionic radii, electronegativity and polarisability are different. In addition, Pb^{2+} and La^{3+} ions have different charge and electronegativity with closed polarisability, but the La^{3+} polarizability, much higher than that of Ca^{2+}, should certainly plays a key role in the distribution of this ion between the two sites. The cationic occupancy of Ca, Pb and La atoms in britholite can be justified based on the large difference in polarizabilities of Ca^{2+} and La^{3+} ions. Ca^{2+} is a hard acid, giving mainly ionic interactions with oxygen, whereas Pb^{2+} and La^{3+} are soft acids, displaying a considerable tendency towards polarization and covalent interactions. On the other hand, F^- is a hard base, having a little affinity for polarizable cations [24,29,30] (Table 4). With increasing Pb^{2+} and La^{3+} content in M(2) sites, it tends to move away from these cations leading to the weakening of the (Ca, La, Pb)-F bond, where the increase of its length favors the structure stability. It seems hence that the Pb^{2+} and La^{3+} polarizability overcomes the steric effect. The notable mobility of the fluoride ion in the presence of polarizable cations has been widely investigated in other studies [11,31].

Table 3

Statistic distribution and refined occupancy of Ca, Pb and La atoms in M(1) and M(2) sites in apatite structure

		Distribution from refinement (A)		Statistic distribution (B)		(A-B/B)	
		M(1)	M(2)	M(1)	M(2)	M(1)	M(2)
$Ca_6Pb_1La_3FAp$							
Ca	5.99	2.786	3.204	2.396	3.594	+0.162	-0.108
Pb	0.996	0.012	0.984	0.398	0.597	-0.969	+0.648
La	2.988	0.804	2.184	1.152	1.792	-0.432	+0.218
$Ca_5Pb_2La_3FAp$							
Ca	5.628	2.294	2.688	2.251	3.376	+0.019	-0.203
Pb	1.992	0.180	1.812	0.796	1.195	-0.773	+0.516
La	2.987	0.887	2.10	1.195	1.792	-0.256	+0.171

Table 4

Radii, electronegativity and polarisability of Ca^{2+}, Pb^{2+} and La^{3+}

	Ca^{2+}	Pb^{2+}	La^{3+}
Radius (Å): coordination no. 6 [24]	1.14	1.33	1.17
Radius (Å): coordination no. 7 [24]	1.20	1.37	1.24
Radius (Å): coordination no. 9 [24]	1.32	1.49	1.35
Polarisability (cm^3 mol^{-1}) [29]	1.59	11.9	13.07
Electronegativity [30]	1.00	1.8	1.1

The (P/Si)-O, M-O, M-M, and M(2)-F interatomic distances are gathered in Table 5. The values of the mean M(1)-O and M(2)-O distances slightly increase when the amount of lead in the fluorobritholite decreases in agreement with the increases of the *a*-axis.

The insertion of lead in the fluorobritholite lattice appreciably affects significantly the fluoride position along the *c*-axis, noting that fluoride is located between the planes of the M(2) triangles (z= ½) of $Pb_{10}(PO_4)_6F_2$ structure. The variation of the M(2)–M(2) distances is significantly larger than what were found for M(1)–M(1) distances. This is due to the increase of the unit cell, with the decrease of lead content, which determines the approach of metal columns, metal triangles and phosphate-silicate ions without a significant structural distortion. For $Ca_5Pb_2La_3$FAp, the average (P,Si)-O distances is significantly smaller than the second phase $Ca_6Pb_1La_3$FAp, while the distance M(1)-O and M(2)-O is significantly larger than that in $Ca_6Pb_1La_3$FAp. A similar phenomenon has been observed for the mixed hydroxyapatite Cd-PbHAp in our previous work [32].

Table 5

Inter-atomic distances (Å) and angles (°) with their standard deviations for $Ca_{7-x}Pb_xLa_3(PO_4)_3(SiO_4)_3F_2$ samples

Formulae	Ca_7La_3FAp	$Ca_6Pb_1La_3$FAp	$Ca_5Pb_2La_3$FAp
(P/Si)-O(1)	1.552(2)	1.620(7)	1.546(7)
(P/Si)-O(2)	1.533(16)	1.506(8)	1.457(5)
(P/Si)-O(3) (×2)	1.608(9)	1.579(2)	1.490(1)
<(P/Si)-O>	1.575	1.569	1.498
O(1)-(P/Si)-O(2)	108.9(8)	109.7(1)	112.1(1)
O(1)-(P/Si)-O(3) (×2)	113.6(4)	111.7(4	111.9(5)
O(2)-(P/Si)-O(3) (×2)	108.8(2)	108.5(2)	106.5(6)
O(3)-(P/Si)-O(3)	102.9(7)	106.5(1)	107.3(6)
<O-(P/Si)-O>	109.4(3	109.1(2)	109.4(9)
[Ca(1)/Pb(1)/La(1)]-O(1) (×3)	2.454(13)	2.385(9)	2.434(9)
[Ca(1)/Pb(1)/La(1)]-O(2) (×3)	2.510(14)	2.504(2)	2.467(4)
[Ca(1)/Pb(1)/La(1)]-O(3) (×3)	2.863(8)	2.847(3)	2.837(1)
<[Ca(1)/Pb(1)/La(1)]-O>	2.609	2.579	2.580
[Ca(2)/Pb(2)/La(2)]-O(1)	2.715(11)	2.801(2)	2.824(5)
[Ca(2)/Pb(2)/La(2)]-O(2)	2.45(2)	2.480(0)	2.569(7)
[Ca(2)/Pb(2)/La(2)]-O(3) (×2)	2.384(7)	2.393(5)	2.464(0)

[Ca(2)/Pb(2)/La(2)]-O(3) (×2)	2.516(8)	2.564(1)	2.603(1)
<[Ca(2/Pb(2)/La(2)]-O>	2.494	2.560	2.615
[Ca(2)/Pb(2)/La(2)]-F	2.403(6)	2.345(9)	2.335(3)
[Ca(1)]- [Ca(1)]	3.486(11)	3.480(9)	3.509(5)
[Ca(1)]- [Ca(2)]	4.000(5)	4.020(1)	4.027(4)
[Ca(2)]- [Ca(2)]	4.065(6)	4.021(4)	4.035(2)

The variation of the X-ray density (theoretical density), apparent density (experimental density) and porosity p with Pb concentration (x) are also reported in table 6. The X-ray density was calculated using the formula [33]:

$$\rho_{\text{th}} = \frac{\text{ZM}}{N_a V}$$

where, Z is the number of molecules per unit cell of the orthorhombic structure, M is the molecular weight of the sample, N_a is the Avogadro's number, V is the volume for a orthorhombic unit cell. The experimental density of the samples was calculated using the formula [33]:

$$\rho_{\text{exp}} = \frac{m}{\pi r^2 h}$$

where m, r and h are respectively the mass, radius and the thickness of the samples. The percentage porosity was calculated using the relation [33]:

$$p = \left(1 - \frac{\rho_{\text{exp}}}{\rho_{\text{th}}}\right) \text{x } 100$$

From table 6, the experimental density of the samples was found smaller than the theoretical density, which may be due to the existence of pores, which in turn, depends on the sintering conditions. Indeed, during pressing of these ceramic powder particles, some pores or void spaces are created. During thermal treatments, a grain boundary forms between adjacent particles and every interstice becomes a pore. The value of the percentage porosity of the samples was found in the range 3 to 25% (see table 6).

Table 6

Values of ρth, ρexp and p of samples $Ca_{7-x}Pb_xLa_3(PO_4)_3(SiO_4)_3F_2$, prepared by solid state reaction.

	ρ_{exp} (g cm^{-3})	ρ_{th} (g cm^{-3})	$\left(\frac{\rho_{exp}}{\rho_{th}}\right)\times 100$	p (%)
x=0	3.789	3.936	96.2	3.7
x=1	3.684	4.256	86.5	13.4
x=2	3.658	4.888	74.8	25.1

3.3. IR investigation

The substitution of calcium by lead reduces the wavenumber IR-bands of (PO_4) and (SiO_4) (Table 7), despite the slight increase in the crystal parameters. This particular development could be explained by the greater polarizability of Pb^{2+}, leading to an increase of the M-O bond covalent character and a weakening of the P-O bond, while Ca^{2+} cations are less polarizable than $Pb^{2+}$where a decrease of covalency of the M-O bond and a strengthening of the P-O bond. It seems that the evolution of the frequencies of the modes of internal vibrations of the anion (PO_4^{3-}) is more influenced by the character of M-O bond, and therefore of the polarizability of M that the evolution of the vibration of the associated cations and crystalline settings.

Table 7

Assignment of the IR absorption bands (cm^{-1}) for the $Ca_{7-x}Pb_xLa_3(PO_4)_3(SiO_4)_3F_2$ samples

	PO_4^{3-}	SiO_4^{4-}

	υ_1	υ_2	υ_3	υ_4	υ_1	υ_2	υ_3	υ_4
$Ca_7La_3F_2$	923	462	1090-1045	598-545	870	409-386	960	500
$Ca_6Pb_1La_3F_2$	921	462	1088-1032	596-545	864	405-382	950	492
$Ca_5Pb_2La_3F_2$	916	460	1090-1040	598-545	865	409-391	956	497

3.4. Electrical properties

Figure 3 shows the conductivity frequency's dependence of $Ca_{7-x}Pb_xLa_3(PO_4)_3(SiO_4)_3F_2$ materials for x=0; 1 and 2. Two characteristic features of σ(ω) behaviour can be noted. A first DC component, independently in frequency, corresponds to the DC conductivity. The second component denoted $\sigma_{AC}(\omega)$ is associated to the dispersive regime at high frequencies given by the following equation: $\sigma_{AC}(\omega) = A\omega^s$. Where A is a temperature-dependent constant, $\omega=2\pi f$ is the angular frequency and "s" is a dimension less critical exponent ($0<s<1$) tightly related to dispersion in polarisation mechanism. Really, lower (s) values are indicative of discontinuous hopping between localized sites at low frequencies [34].

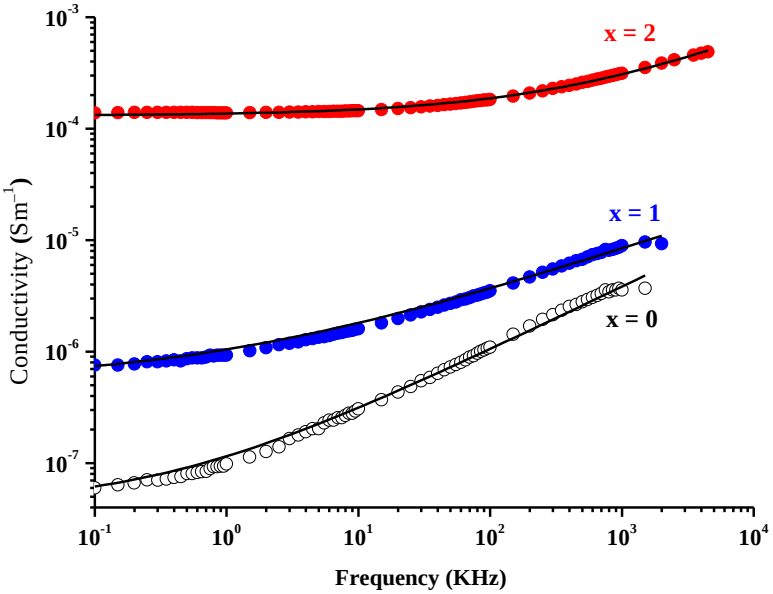

Figure 3. Frequency dependent of conductivity spectra of $Ca_{7-x}Pb_xLa_3(PO_4)_3(SiO_4)_3F_2$ for x= 0, 1 and 2. Plain lines (—) correspond to the simulation of experimental data.

The fitting results of different devices are summarized in Table 8. From σ_{DC}, s and A values, the hooping frequency is defined as $f_H = \left(\frac{\sigma_{DC}}{A}\right)^{\frac{1}{s}}$, which can also determine the hooping time; the necessary time for an ion to hop from i to j site; related to hooping frequency defined by: $\tau_{ij} = \frac{1}{f_{ij}}$ [35].

Table 8

Electrical parameters for $Ca_{7-x}Pb_xLa_3(PO_4)_3(SiO_4)_3F_2$ materials

	x=0	x=1	x=2
σ_{DC}(S m^{-1})	4.21×10^{-8}	5.38×10^{-7}	1.30×10^{-4}
A	7.31×10^{-8}	5.08×10^{-7}	5.78×10^{-6}
s	0.571	0.387	0.495
f_H(KHz)	0.380	1.159	538.696

The increase of σ_{DC} versus Pb content in substituted fluorobritholites with a decrease in the hooping time indicates that the fluoride hop became faster. So, the introduction of Pb^{2+} in fluorobritholite structure enhances the fluoride mobility with a large $\sigma_{DC}(x=2)/\sigma_{DC}(x=0)$ ratio of 3×10^3, related to the priority occupation of Pb in M(2) sites, where the fluorine has affected by the Pb and La substitutions. To better clarify the conduction properties of these fluorobritholite materials, the figure 4 shows the frequency dependent of the real and imaginary parts of the complex impedance for $Ca_{7-x}Pb_xLa_3(PO_4)_3(SiO_4)_3F_2$ compounds measured at room temperature.

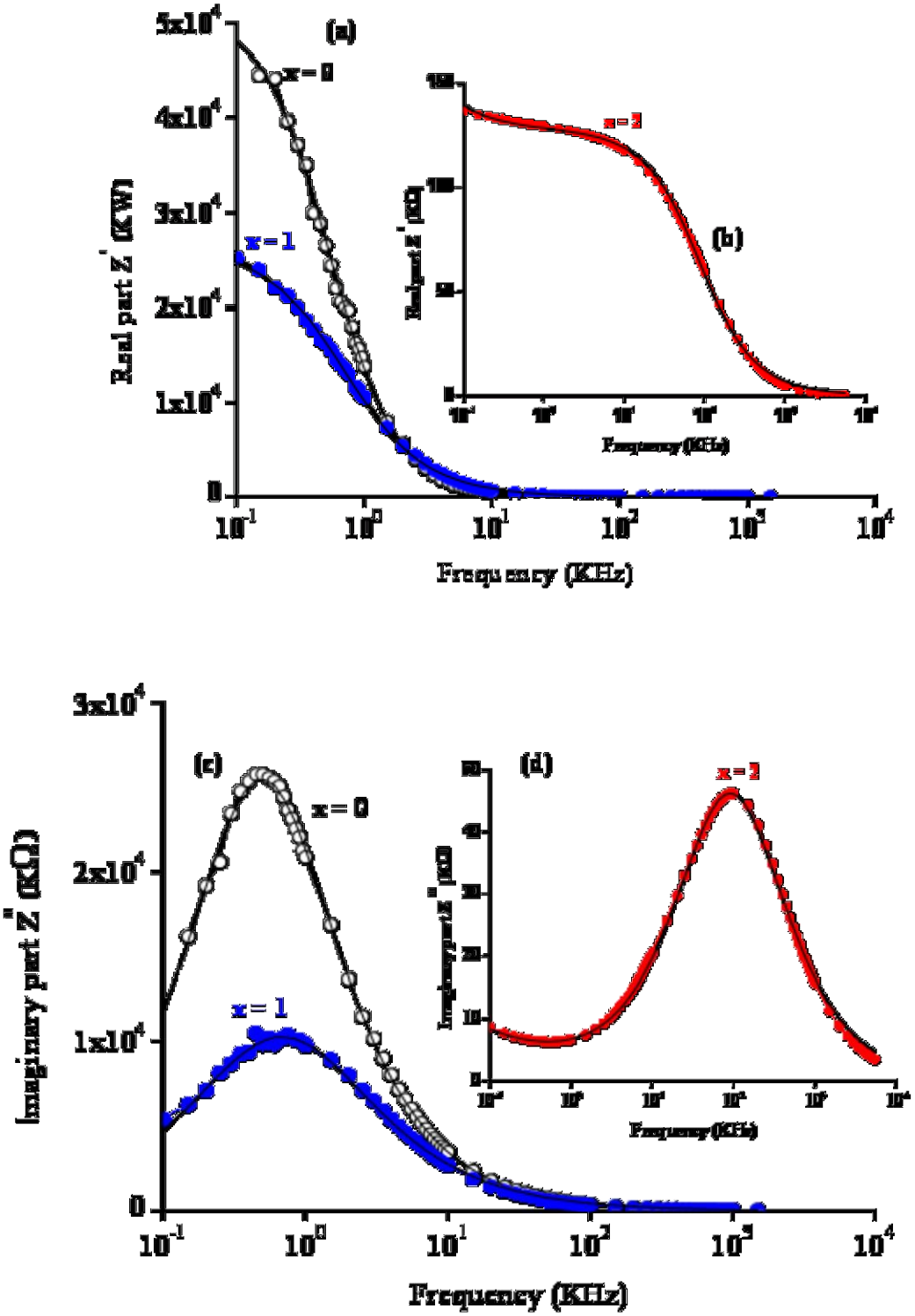

Figure 4. (a, b) Real and (c, d) imaginary parts of complex impedance for $Ca_{7-x}Pb_xLa_3(PO_4)_3(SiO_4)_3F_2$ (x =0 , 1 and 2). Plain lines (—) correspond to the simulation of experimental data.

The evolution of Z' and Z" parts with the corresponding frequency exhibits a distribution of relaxation times intrinsically related only one relaxation with the real part Z' is more affected by the substitution rate x (Ca→Pb) in fluorobritholite structure. The high polarizability of Pb and the widening tunnels by the introduction of the big cations favor the fluoride mobility from the occupied site to the vacant site in a one-dimensional channel.

Cole-Cole plots for the three substituted fluorobritholite materials are shown in figure 5. All curves show a single semi-circle at high frequencies characterized by a RC circuit (R_1//C $_{CPE1}$). For x=2, a second semi-circle at low frequencies is observed related to high charge mobility at interface, corresponding a second equivalent circuit (R_2//C_{CPE2}). These equivalent circuits are inset in figure 4, and their parameters are presented in the table 9.

The CPE impedance (Z_{CPE}) is given by the following relation:

$$Z_{\mathrm{CPE}} = \frac{1}{A_0 (j\omega)^n}$$

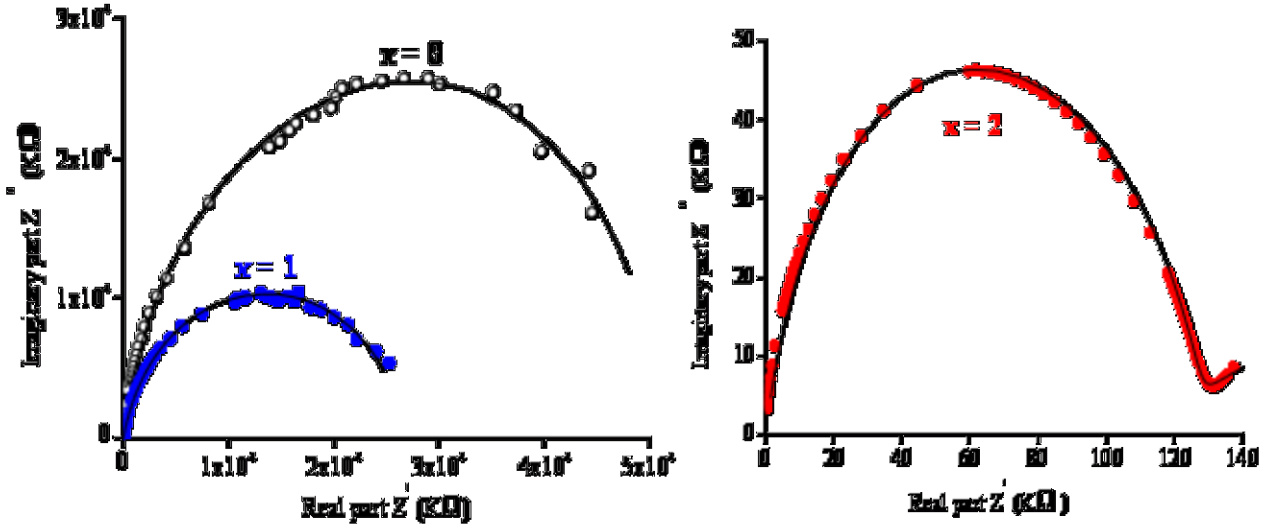

where n ($0 < n < 1$) is the exponent which determines a constant phase angle equal to ($n\pi/2$), $\omega = 2\pi f$is the angular frequency, $j^2 = -1$ and A_0 is the CPE parameter (expressed in Farad

units). For an *n* value equal to 1, 0.5 or 0, CPE will be, respectively, an ideal capacitance, a Warburg impedance or an ideal resistance.

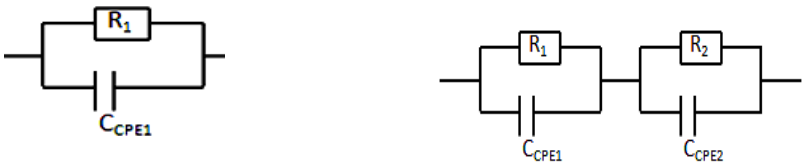

Figure 5. Cole-Cole plots of $Ca_{7-x}Pb_xLa_3(PO_4)_3(SiO_4)_3F_2$ for x=0, 1 and 2. Plain lines (—) correspond to the simulation of experimental data. These inset show the equivalent circuits.

Table 9

Equivalent circuit electrical parameters for $Ca_{7-x}Pb_xLa_3FAp$

	$R_1(M\Omega)$	$C_{CPE1}(\mu F)$	n_1	$\tau_1(ms)$	$R_2(M\Omega)$	$C_{CPE2}(nF)$	n_2	$\tau_2(ms)$
Ca_7La_3FAp	51.605	34.92	0.923	1.976	-	-	-	-
$Ca_6Pb_1La_3FAp$	26.847	52.23	0.920	1.218	-	-	-	-
$Ca_5Pb_2La_3FAp$	0.128	14.72	0.894	0.018	254.32	6.02	0.891	1.524

The device resistance decreases with the Pb content in $Ca_{7-x}Pb_xLa_3FAp$ structure as well as hopping time. We note an increase in relaxation frequency and a decrease in relaxation time with inserted Pb and the electrical response of fluorobritholite materials became faster. The ionic conductivities σ of the substituted-fluorobritholite materials at room temperature are calculated from Cole-Cole plots using the relation σ=e/RS where e and S are the thickness and

electrode surface of the sample, respectively. The bulk resistance R was deduced from the high-frequency intersection of the semi-circle with the real axis. The DC conductivity value for $Ca_5Pb_2La_3(PO_4)_3(SiO_4)_3F_2$ (x=2) material at room temperature is $\sigma_{DC} = 1\times10^{-4}$ S m^{-1} lower than that of x=1 ($\sigma_{DC} = 4.74\times10^{-7}$ S m^{-1}) and x=0 ($\sigma_{DC} = 2.46\times10^{-7}$ S m^{-1}). The better ionic conductivity is observed particularly for *x*=2. In fact, the large interface impedance with electrodes characterized by a straight line at low frequencies and the higher conductivity value of $Ca_5Pb_2La_3(PO_4)_3(SiO_4)_3F_2$ compared with those of $Ca_6Pb_1La_3(PO_4)_3(SiO_4)_3F_2$ and $Ca_7La_3(PO_4)_3(SiO_4)_3F_2$ ($\sigma_{x=2}/\sigma_{x=0} \approx 4\times10^{+2}$) provide an important fluoride mobility while the Pb atoms are introduced in fluorobritholite structure.

Conclusion

A series of fluorobritholites $Ca_{7-x}Pb_xLa_3(PO_4)_3(SiO_4)_3F_2$ ($0\leq x\leq 2$) was prepared by using a solid-state reaction and investigated by the X-ray diffraction. A structural investigation indicated that all these compounds adopt the $P6_3/m$ space group structure. The refinement of the occupation factors indicates that the tree metallic ions Ca^{2+}, Pb^{2+} and La^{3+} are distributed between the two crystallographic sites M(1) and M(2), with preference of lead and lanthanide for the M(2) site. At low concentrations, Pb occupies almost exclusively the M(2) site. The IR spectroscopy indicated that the substitution of PO_4^{3-} by SiO_4^{4-} group was successfully performed. Conductivity measurements and impedance spectroscopy show an improvement in conductivity and a weakness in response time while adding Pb ions indicating that the addition of Pb improve the electrical properties of fluorobriholite material.

Acknowledgments

The authors gratefully Mr Ali HADROUG for the English Language assistance. We gratefully acknowledge University of Monastir and Kairouan, (Tunisia); the University Pierre and Marie Curie and CNRS (France) for the financial support.

References

[1] K. Boughzala, E. Ben Salem, F. Kooli, P. Gravereau, K. Bouzouita, Spectroscopic studies and Rietveld refinement of strontium-britholites. J. Rare Earth. 26 (2008) 483-488.

[2] K. Boughzala, K. Bouzouita. Synthèse et caractérisation de strontium-calcium-lanthane apatites $Sr_{7-x}Ca_xLa_3(PO_4)_3(SiO_4)_3F_2$ $0 \leq x \leq 2$, C. R. Chimie 18 (2015) 858-866.

[3] K. Boughzala, E. Ben Salem, A. Ben Chrifa, E. Gaudin, K. Bouzouita, Synthesis and characterization of strontium–lanthanum apatites. Mater. Res. Bull. 42 (2007) 1221-1229.

[4] M. Zahouily, Y. Abrouki, A. Rayadh, S. Sebti, H. Dhimane, M. David. Fluorapatite: efficient catalyst for the Michael addition. Tetrahedron Lett. 44 (2003) 2463-2465.

[5] S. M. Hosseini, T. Shvareva, A. Navrotsky. Energetics of lanthanum silicate apatite: Influence of interstitial oxygen and cation vacancy concentrations in $La_{9.33+x}(SiO_4)_6O_{2+3x/2}$ and $La_{10-x}Sr_x(SiO_4)_6O_{3-0.5x}$. Solid State Ionics 233 (2013) 62-66.

[6] K. Liu, L.B. Liao, J. Chen, Q.F. Guo, Y. Zhang, L.F. Mei. Tunable luminescence properties and energy transfer of $Ba_3NaLa(PO_4)_3F$:Tb,Sm phosphors with apatite structure J. Lumin. 169 (2016) 739-743.

[7] B. H. Yoon, H.W. Kim, S.H. Lee, C.J. Bae, Y.H. Koh, Y.M. Kong, H.E. Kim. Stability and cellular responses to fluorapatite-collagen composites. Biomater. 26 (2005) 1050- 2957.

[8] M. I. Kay, R. A. Young, A. S. Posner. Crystal structure of hydroxyapatite. Nat. 204 (1964) 1050-1052.

[9] Mc Donnell D. Apatite, Its Crystal Chemistry, Mineralogy, Utilization, and Geologic and Biologic Occurrences, Springer, New York, N. Y., 1973.

[10] A. Laghzizil, N. Elhrech, O. Britel, A. Bouhaouss, M. Ferhat. Removal of fluoride from moroccan phosphate and synthetic fluoroapatites. J. Fluorine Chem. 101 (2000) 69-73.

[11] A. Laghzizil, A. Bouhaouss, M. Ferhat, P. Barboux, R. Morineau, J. Livage. Anionic conductivity in fluorapatites : correlation between structure and electrical properties. Adv. Mat. Res. 1 (1994) 479-488.

[12] A. Laghzizil, A. Bouhaouss, P. Barboux, R. Morineau, J. Livage. Mixed ionic conductivities in sodium fluoroapatites. Solid State Ionics 67 (1993) 137-143.

[13] A. Laghzizil, S. El Hajjaji, A. Bouhaouss, M. Ferhat. Ionic conductivities of lithium fluorapatites. Solid State Ionics 126 (1999) 245-250.

[14] A. Laghzizil, P. Barboux, A. Bouhaouss. Cationic conductivity and structural studies in the $Pb_8K_{2-x}Na_x(PO_4)_6$ system. Solid State Ionics 128 (2000) 177- 181.

[15] S. Nakayama, H. Aono, Y. Sadaok. Ionic conductivity properties of $Ln_{10}(SiO_4)_6O_3$ (Ln=Na, Nd, Sm, Gd and Dy. Chem. Lett. 24 (1995) 431-442.

[16] H. Arikawa, H. Nishiguchi, T. Ishihara, Y. Takita. Oxide ion conductivity in Sr-doped $La_{10}Ge_6O_{27}$ apatite oxide. Solid State Ionics 136 (2000) 31-37.

[17] J. E. H. Sansom, D. Richings, P. R. Slater. A powder neutron diffraction study of the oxide-ion-conducting apatite-type phases, $La_{9.33}Si_6O_{26}$ and $La_8Sr_2Si_6O_{26}$. Solid State Ionics 139 (2001) 205-2010.

[18] L. Boyer, J. Carpena, J.L. Lacout. Synthesis of phosphate-silicate apatites at atmospheric pressure. Solid State Ionics 95 (1998) 121-129.

[19] C. Meis, J.D. Gale, L. Boyer, J. Carpena, J. Grosset. Theoretical Study of Pu and Cs Incorporation in a Mono-silicate Neo-dymium Fluoroapatite $Ca_9Nd(SiO_4)(PO_4)_5F_2$. J. Phys. Chem. 104 (2000) 5380-5387.

[20] H. Njema, M. Debbichi, K. Boughzala, M. Said, K. Bouzouita. Structural, electronic and thermodynamic properties of britholites $Ca_{10-x}La_x(PO_4)_{6-x}(SiO_4)_xF_2$ ($0 \leq x \leq 6$): Experiment and theory. Mater. Res. Bull. 51 (2014) 210-2016.

[21] H. M. Rietveld. Profile refinement method for nuclear and magnetic structures J. Appl. Crystallogr. 2 (1969) 65–71.

[22] J. Rodriguez-Carvajal, FULLPROF: a program for Rietveld refinement and pattern matching analysis, In: Collected Abstract of Powder Diffraction Meeting, Toulouse, France, vol. 127, 1990.

[23] N. Leroy, E. Bres. Structure and substitution in fluoroapatite. Eur. Cells Mate. 2 (2001) 36-48.

[24] R. D. Shannon. Revised effective ionic radii and systematic studies of interatomic distances in halides and chalcogenides. Acta Crystallogr. A32 (1976) 751-767.

[25] K. Boughzala, M. Debbichi, H. Njema, K. Bouzouita. Rietveld refinement, electronic structure and ionic conductivity of $Sr_4La_6(SiO_4)_6F_2$ and $Sr_4La_6(SiO_4)_6O$ ceramics. J. Solid State Chem. 239 (2016) 84-90.

[26] K. Boughzala, S. Nasr, E. Ben Salem, F. Kooli, K. Bouzouita. Structural and spectroscopic investigation of lanthanum-substituted strontium-oxybritholites. J. Chem. Sci. 121 (2009) 283-291.

[27] K. Ardhaoui, M.V. Coulet, A. Ben Cherifa, J. Carpena, J. Rogez, M. Jemal. Standard enthalpy of formation of neodymium fluorbritholites. Thermochem. Acta. 444 (2006) 190-194.

[28] K. Ardhaoui, J. Rogez, A. Ben Chérifa, M. Jemal, P. Satre. Standard enthalpy of formation of lanthanum oxybritholites. J. Therm. Anal. Calorim. 86 (2006) 553-559.

[29] Y. Marcus. Ion Properties, Marcel Dekker, New York, 1997.

[30] D. R. Lide (Ed.), Handbook of Chemistry and Physics, 79th ed., CRC, Boca Raton, 1998.

[31] A. Laghzizil, N. El Herch, A. Bouhaouss, G. Lorente, J. Macquete. Comparison of Electrical Properties between Fluoroapatite and Hydroxyapatite Materials. J. Solid State Chem. 156 (2001) 57-60.

[32] B. Badraoui, A. Bigi, M. Debbabi, M. Gazzano, N. Roveri, R. Thouvenot. Physicochemical Properties and Structural Refinement of Strontium-Lead Hydroxyapatites. Eur. J. Inorg. Chem. 7 (2002) 1864-1870.

[33] K. M. Batoo, S. Kumar, C. G. Lee, Alimuddin, Influence of Al doping on electrical properties of Ni-Cd nano ferrites. Curr. Appl. Phys. 9 (2009) 826-832.

[34] K. Jonscher, The 'Universal' Dielectric Response. Nat. 267 (1977) 673-679.

[35] P. S. Anantha, K. Hariharan. AC Conductivity analysis and dielectric relaxation behaviour of $NaNO_3$-Al_2O_3 composites. Mater. Sci. Eng. B121 (2005) 12-19.